A Test Model of a Power Grid with Battery Energy Storage and Wide-Area Monitoring

Lianfang Cai, Nina F. Thornhill, *Senior Member, IEEE*, Stefanie Kuenzel, *Member, IEEE*, Bikash C. Pal, *Fellow, IEEE*

***Abstract*—This paper presents a test model for investigating how to coordinate a power grid and Energy Storage Systems (ESSs) by Wide-Area Monitoring (WAM). It consists of three parts: (1) a model of a power grid containing different types of generators, loads and transmission network; (2) a model of lithium-ion battery ESSs; (3) a model of multivariate statistical analysis based WAM built to capture the grid information for guiding the operation of ESSs. Simulation studies using a reduced equivalent model specifically built for a UK power grid enhanced with lithium-ion battery ESSs and WAM illustrate the way in which WAM can coordinate a power grid and ESSs, and also demonstrate the benefit of ESSs on a power grid.**

***Index Terms*—Power grid, wide-area monitoring, lithium-ion battery, energy storage, multivariate statistical analysis, model.**

I. Introduction

LIKE many other countries around the world, the United Kingdom (UK) is committed to reduce the utilization of fossil fuels and the emissions of CO_2. In the Climate Change Act 2008 [1], a goal to ensure that the net UK emissions of green-house gases for the year 2050 are at least 80% lower than the 1990 baseline was set up. Subsequently, in the Directive 2009/28/EC of the European Parliament and of the Council of the European Union [2], a target was defined for the UK that 15% of its total energy consumption from renewable sources should be achieved by 2020. In the Electricity Ten Year Statement 2016 published by National Grid recently [3], this target was stated again. In line with the above legislations, the generation patterns in the UK are evolving rapidly, characterized by a decreasing volume of conventional thermal generation from coal and gas but an increasing volume of renewable generation largely in the form of offshore wind generation and asynchronously connecting to the transmission network [4].

Many renewable energy resources are intermittent in nature. Such intermittency presents a great challenge in maintaining the balance between generation and demand, and thus it has detrimental effects on power grid security and stability [5]-[8]. In this situation, Energy Storage Systems (ESSs) can play an important role in managing the fluctuations of electricity generated from renewable energy resources [9]-[11]. With the introduction of ESSs, more renewable energy resources can be incorporated to aid the transition to the low-carbon and clean power generation.

Although ESSs can facilitate renewable generation well, the integration of ESSs into a power grid is a complex task, involving investigation of two major issues: the ESSs planning and the ESSs control. The ESSs planning includes the storage type selection, sizing and siting. Usually, the storage type selection depends on the technical features of ESSs and the application services ESSs are supposed to provide. For instance, for energy management, a storage type with large-scale energy capacity such as battery storage or pumped hydro storage is often more appropriate, while for power quality improvement, a storage type with fast response and small energy capacity such as superconducting magnetic storage or super-capacitor storage is often more suitable. The storage sizing usually refers to the determination of the power rating and the energy rating and it can be obtained by balancing the benefits and cost [6]. Recently, methods for optimizing the storage sizing and siting have been proposed. Wogrin and Gayme [12] presented a DC optimal power flow (OPF) framework for storage portfolio optimization, where the optimal storage siting and operation given a fixed portfolio of different storage types were decided and the optimal storage portfolio in terms of the storage type, sizing and siting was subsequently determined. Pandžić *et al*. [13] presented a near-optimal method for the storage siting and sizing problem by considering both the economic and technical aspects of the problem and conducting a three-stage decomposition of the problem. Dvorkin *et al*. [14] presented a bilevel program for determining the optimal storage sizing and siting, which can reduce the system-wide operating cost and the cost of investments in storage while ensuring that ESSs collect sufficient profits to fully recover their investment cost.

The ESSs control is demanded for providing application services to a power grid. There are many application services ESSs can provide to a power grid, such as transmission congestion relief, grid stabilization, emergency power supply, frequency regulation, and so on [6]. Different application services usually have different requirements for the ESSs operation and control, and therefore, the ESSs operation and control

This work was supported by the U.K. Engineering and Physical Sciences Research Council under Grant "EP/L014343/1" "Stability and Control of Power Networks with Energy Storage (STABLE-NET)."

L. Cai and N. F. Thornhill are with the Centre for Process Systems Engineering, Department of Chemical Engineering, Imperial College London, SW7 2AZ, U.K. (e-mail: l.cai@imperial.ac.uk; n.thornhill@imperial.ac.uk).

S. Kuenzel is with the Department of Electronic Engineering, Royal Holloway, University of London, TW20 0EX, U.K. (e-mail: stefanie.kuenzel@rhul.ac.uk).

B. C. Pal is with the Department of Electrical and Electronic Engineering, Imperial College London, SW7 2AZ, U.K. (e-mail: b.pal@imperial.ac.uk).

vary with application services. Almassalkhi *et al.* [15] considered incorporating ESSs as a flexible transmission asset and presented a three-level framework to coordinate day-ahead, near real-time and minute-by-minute control actions of conventional generation and ESSs. Martin and Hiskens [16] proposed a corrective model-predictive control algorithm to coordinate the response of controllable resources including ESSs that can limit detrimental effects of contingencies and identify beneficial control actions across a wide range of devices. Khani *et al.* [17] proposed a real-time optimal dispatch algorithm for ESSs that can generate revenue by exploiting electricity price arbitrage opportunities in the day-ahead electricity market while optimally preparing ESSs to maximize their contribution to congestion relief. Farraj *et al.* [18] investigated the role of ESSs in stabilizing the dynamics of power systems during periods of disruption, considered an information-rich multiagent framework and focused on ESS output control via linear feedback optimal control to achieve transient stability. Choi *et al.* [19] built a hybrid operation strategy for a wind energy conversion system with a battery ESS that can improve the frequency regulation capability of the studied power system.

Besides the above analyzed works, there exists a large body of research investigating the ESSs planning, operation and control, e.g., [20]-[25]. These activities exploit the merits of ESSs for specific application purposes and provide significant reference for incorporating ESSs to a power grid. Although ESSs can provide attractive services to the power grid operation as demonstrated by the existing research, an important premise is that the grid information can be effectively captured to guide the operation of ESSs. For instance, the output power of wind turbines in a certain area may be excessive during high wind periods or low when there is little wind. If there is no available information about when and where the event of excessive or scant wind generation occurs, ESSs in different areas will react to an excess of wind power by charging, or react by discharging if there is insufficient wind power. This will cause a significant power flow change across a power grid, compromising the grid operational stability margin. This will also cause a waste of limited storage resource since ESSs are usually an expensive investment and it is not economically viable for all ESSs to work for a single application service [6]. On the contrary, if this event can be detected and located, the obtained information can enable a response in which only ESSs near the target area charge or discharge and ESSs in other locations can await orders for other application services, resulting in a reduced impact on the grid stability and an economical utilization of ESSs.

However, to the best of authors' knowledge, the existing research on the integration of ESSs into a power grid seldom investigate how to coordinate a power grid and ESSs by capturing the grid information. The motivation of this work is thus to fill this gap by developing a Wide-Area Monitoring (WAM) method based on multivariate statistical analysis. The developed WAM method can detect and locate events in a power grid to guide the operation of ESSs centrally, which also responds to the proposition in [26] combining dispersed ESSs as a virtual storage unit and controlling centrally. A further motivation is to build a test model of a power grid enhanced with both ESSs and WAM. The overall framework of this test model is shown in Fig. 1, illustrating a system configuration of a power grid, battery ESSs, and WAM. Such a test model is of importance to academic research, since it can simulate practical scenarios to provide insights into the way in which WAM can coordinate a power grid and ESSs as well as how a power grid can benefit from ESSs with the support of WAM.

The paper is organized as follows. Section II gives a description of a power grid model. Section III describes a model of lithium-ion battery ESSs. Section IV presents a model of multivariate statistical analysis based WAM. The simulation results and analysis using a test model specifically built for a UK power grid enhanced with lithium-ion battery ESSs and WAM are provided in Section V, while the conclusions are drawn in Section VI.

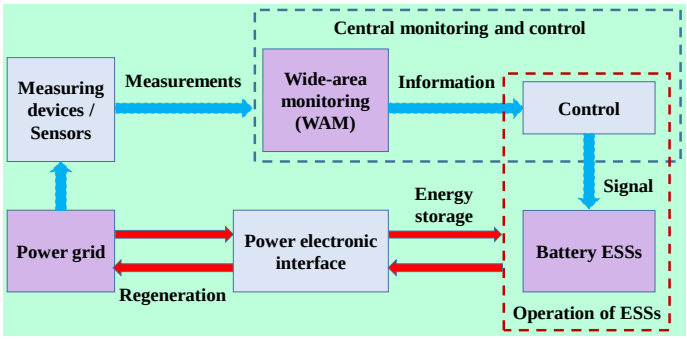

Fig. 1. The overall framework of the built test model.

II. A Power Grid Model

This section describes a model of a power grid including different types of generators, loads and transmission lines.

A. Generation mix

Here, the generation based on coal, nuclear, Combined Cycle Gas Turbine (CCGT), hydro, onshore wind and offshore wind is taken into account. The combined heat and power capacity and biomass capacity are added to the coal capacity, while the tidal and wave capacities are added to the offshore wind capacity. The reason is that these added capacities are usually not significant enough to be represented separately. The oil based generation and the gas based generation are grouped together because they have similar dynamic characteristics. Besides, an important assumption is the aggregation of wind farms where several wind farms located in one site are viewed as one wind turbine generator. The synchronous machines are represented by a transient model and the recommended ranges of values for different generator parameters are obtained from [27]. Each synchronous machine is accompanied by a governor that is also modelled according to [27]. The wind turbine generators are represented by the generic Type-4 WTG model [28].

B. Load demand

The active power and the reactive power of demand at the ith load bus for $i = 1,2,\cdots$ are respectively represented as [27]:

$$p_{\mathrm{L}_i} = p_{\mathrm{L}_i,0}\left(\frac{v_{\mathrm{L}_i}}{v_{\mathrm{L}_i,0}}\right)^a \quad (1)$$

$$q_{\mathrm{L}_i} = q_{\mathrm{L}_i,0}\left(\frac{v_{\mathrm{L}_i}}{v_{\mathrm{L}_i,0}}\right)^b \quad (2)$$

where v_{L_i} denotes the voltage magnitude of the ith load bus L_i, while $p_{\mathrm{L}_i,0}$, $q_{\mathrm{L}_i,0}$ and $v_{\mathrm{L}_i,0}$ denote the initial values of p_{L_i}, q_{L_i} and v_{L_i}, respectively. The parameter a in (1) is set to 1 assuming that the active component of load has constant current characteristic, while the parameter b in (2) is set to 2 assuming that the reactive component of load has constant impedance characteristic [27]. Moreover, Gaussian noise is added into p_{L_i} and q_{L_i} so that the continuous random load perturbations observed in the actual power grid can be represented.

C. Transmission network

The transmission network with its overhead lines and cables is represented by the impedance matrix [27].

III. Model of Lithium-Ion Battery ESSs

This section describes a model of lithium-ion battery ESSs, referred to as LIBESS. The elementary unit of LIBESS is a Lithium-Ion Battery Cell (LIBC) model presented in [29]. This cell model was validated based on a current profile derived from the Artemis drive cycle [30] by differentiating the speed vector and scaling the profile to the desired maximum current.

In the following, LIBC is described firstly to lay the foundation for the subsequent presentation of LIBESS. More details about LIBC can be found in [29].

LIBC was designed to simulate the terminal voltage response of a lithium-ion battery cell to any arbitrary current input over a range of temperatures, states of charge (SOCs) and C-rates, where C-rates refer to the rates at which a battery cell is charged or discharged. The model order of LIBC was determined by minimizing the loss function of the state space equation when fitted to the voltage measurements of the current pulse experiments. In [29], the minimization was carried out for a model order from one to five and for data recorded between 0 °C and 50 °C at every SOC. For the majority of the recorded data (10% <= SOCs <= 90%), the optimal model order was two. It was thus chosen for LIBC. The equivalent circuit of LIBC is shown in Fig. 2 and the corresponding state space model is:

$$\begin{bmatrix}\dot{V}_1\\ \dot{V}_2\end{bmatrix} = \begin{bmatrix}-\frac{1}{R_1C_1} & 0\\ 0 & -\frac{1}{R_2C_2}\end{bmatrix}\begin{bmatrix}V_1\\ V_2\end{bmatrix} + \begin{bmatrix}\frac{1}{C_1}\\ \frac{1}{C_2}\end{bmatrix} I_{\mathrm{cell}} \quad (3)$$

$$V_{\mathrm{cell}} = V_{\mathrm{OC}} + V_1 + V_2 + R_0 I_{\mathrm{cell}} \quad (4)$$

where two resistor-capacitor parallel branches (R_1//C_1, R_2//C_2) connected in series account for diffusion, the resistor R_0 consists of ohmic and charge transfer resistance, V_1 and V_2 are the potential voltage differences across the elements R_1//C_1 and R_2//C_2 respectively, I_{cell} is the cell current serving as the model input, and V_{cell} is the cell terminal voltage serving as the model output, while V_{OC} is the open circuit voltage.

Next, LIBESS is directly built based on LIBC by assuming that the cells in a lithium-ion battery ESS are identical and there is no significant intrinsic difference (imbalance) among the cells. The active power of LIBESS is then calculated based on the active power of LIBC as the following equation:

$$P_{\mathrm{ESS}} = N \cdot P_{\mathrm{cell}} = N \cdot (V_{\mathrm{cell}} \cdot I_{\mathrm{cell}}) \quad (5)$$

where N is the number of cells in an ESS, which is supposed to be in an appropriate range so that the requirements of energy storage and regeneration can be effectively met.

Although the full battery pack model is a major undertaking, the simplified model (5) can be used conveniently because of its good scalability and can already illustrate that battery ESSs have considerable benefit on the stability of a power grid. Before the utilization of this model, a point worth noting is the determination of ESSs locations in a power grid. Here, an assumption is taken that ESSs are placed close to renewable energy resources (for the test model built in this paper, it is wind energy), so that the intermittency effect of wind energy can be easily relieved.

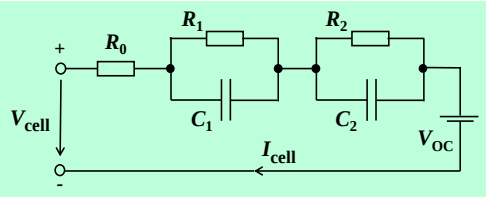

Fig. 2. The model structure of LIBC [29].

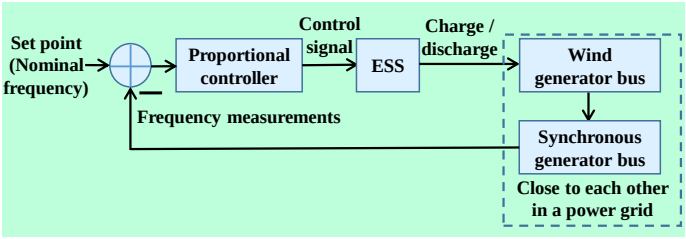

Fig. 3. The control scheme for an ESS.

It is assumed that ESSs connected to wind generator buses satisfy two conditions:

1) ESSs take the frequencies of synchronous generator buses as control objective variables (i.e., the variables to be controlled at their set point values) since frequency control is important for the stability of a power grid [31] and the controller output signal for adjustment of charge or discharge of ESSs are all calculated using a proportional control strategy. The synchronous generator buses whose frequencies are taken as control objective variables are chosen as those close to wind generator buses to which ESSs are connected. The control scheme for an ESS is shown in Fig. 3, where the power electronic interfacing an ESS and a wind generator bus is simply viewed as a switch due to its fast response time that can often be negligible. Denoting $v_{\mathrm{w}_i} = v_{\mathrm{w}_i,\mathrm{real}} + jv_{\mathrm{w}_i,\mathrm{imag}}$ as the voltage at the ith wind generator bus W_i, the current provided by the ith ESS (ESS_i) that is connected to W_i can then be calculated as follows:

$$curr_{\mathrm{ESS}_i} = \frac{v_{\mathrm{w}_i,\mathrm{real}} P_{\mathrm{ESS}_i}}{v^2_{\mathrm{w}_i,\mathrm{real}} + v^2_{\mathrm{w}_i,\mathrm{imag}}} + j\frac{v_{\mathrm{w}_i,\mathrm{imag}} P_{\mathrm{ESS}_i}}{v^2_{\mathrm{w}_i,\mathrm{real}} + v^2_{\mathrm{w}_i,\mathrm{imag}}} \quad (6)$$

where P_{ESS_i} denotes the active power of ESS_i, and j denotes the complex operator, that is, $j^2 = -1$.

2) The controller output signal can be calculated within the measuring period of measurement units and it is kept constant until the next measuring period comes.

The above control strategy ensures that ESSs supply power if the controlled frequencies drop, store power if the controlled

frequencies rise, and thus reduce the frequency nadir or peak.

IV. Model of Multivariate Statistical Analysis based Wide-Area Monitoring

To maximize the role of ESSs in mitigating the intermittency problem of renewable generation in a power grid, the coordination between the power grid and ESSs is of importance. That is, a central monitoring unit of the power grid should be able to tell ESSs when and where electrical energy needs to be stored or returned back. Thus, this section develops a WAM method that includes event detection and event localization based on multivariate statistical analysis known as Principal Component Analysis (PCA) to fulfil this task. The approach can capture the grid information for guiding the operation of ESSs and its details are presented below.

A. Event Detection

Event detection can provide the time when electrical energy needs to be stored by ESSs or returned back to a power grid.

Considering the fact that the frequencies of synchronous generator buses are directly affected by active power and frequency control is usually performed by the real-time balance between active power generation and demand, the active power at a bus is used as a monitored variable here. Denoting p_{S_i}, p_{W_i} and p_{L_i} as the active power at the ith synchronous generator bus S_i, the ith wind generator bus W_i and the ith load bus L_i respectively, the vector of monitored variables is constituted as:

$$\begin{aligned}\boldsymbol{p}^{\mathrm{T}} &= \left[p_{\mathrm{S}_1}\ p_{\mathrm{S}_2}\ \cdots\ p_{\mathrm{S}_{m_{\mathrm{S}}}}\ p_{\mathrm{W}_1}\ p_{\mathrm{W}_2}\ \cdots\ p_{\mathrm{W}_{m_{\mathrm{W}}}}\ p_{\mathrm{L}_1}\ p_{\mathrm{L}_2}\ \cdots\ p_{\mathrm{L}_{m_{\mathrm{L}}}}\right] \\ &= [p_1\ p_2\ \cdots\ p_m] \end{aligned} \tag{7}$$

where $^{\mathrm{T}}$ denotes the vector or matrix transpose operator, m_{S}, m_{W} and m_{L} denote the number of synchronous generator buses, wind generator buses and load buses respectively, $p_1\ p_2\ \cdots\ p_m$ denote the monitored variables sequentially for the convenience of description, and $m = m_{\mathrm{S}} + m_{\mathrm{W}} + m_{\mathrm{L}}$.

Historical recordings of N measurements of active power in the ambient condition are used as the modelling data $\{\boldsymbol{p}_n\}_{n=1}^{N}$, where $\boldsymbol{p}_n{}^{\mathrm{T}} = \left[p_{1,n}\ p_{2,n}\ \cdots\ p_{m,n}\right]$ and $p_{i,n}$ denotes the value of the ith monitored variable p_i at the nth sampling time point for $i = 1,2,\cdots,m$. In what follows, PCA is used to analyze the monitored variables together and to obtain feature variables called Principal Components (PCs) and residual variables (RVs) through multivariate analysis.

Firstly, the monitored variables in the vector $\boldsymbol{p}$ are normalized with the sample means and sample variances calculated from the modelling data $\{\boldsymbol{p}_n\}_{n=1}^{N}$ to make the obtained variables independent of their engineering units. The symbol $\tilde{\boldsymbol{p}}^{\mathrm{T}} = [\tilde{p}_1\ \tilde{p}_2\ \cdots\ \tilde{p}_m]$ denotes the vector of the normalized variables.

The covariance matrix $\boldsymbol{C}$ of $\tilde{\boldsymbol{p}}$ can be estimated based on the normalized modelling data $\{\tilde{\boldsymbol{p}}_n\}_{n=1}^{N}$ and the eigenvalue decomposition of $\boldsymbol{C}$ can be written as:

$$\boldsymbol{C} = \frac{1}{N-1}\sum_{n=1}^{N}\tilde{\boldsymbol{p}}_n\tilde{\boldsymbol{p}}_n^{\mathrm{T}} = \boldsymbol{U}\boldsymbol{\Lambda}\boldsymbol{U}^{\mathrm{T}} = \sum_{i=1}^{m}\lambda_i\boldsymbol{u}_i\boldsymbol{u}_i^{\mathrm{T}} \tag{8}$$

where $\boldsymbol{\Lambda}$ is a diagonal matrix with the diagonal elements as the eigenvalues $\lambda_1, \lambda_2, \cdots, \lambda_m$ of $\boldsymbol{C}$ in the descending order, and $\boldsymbol{U} = [\boldsymbol{u}_1\ \boldsymbol{u}_2\ \cdots\ \boldsymbol{u}_m]$ is the eigenvector matrix with the column vectors as the eigenvectors of $\boldsymbol{C}$.

Based on the matrix $\boldsymbol{U}$, a vector of PCs can be obtained by:

$$\boldsymbol{g}^{\mathrm{T}} = [g_1\ g_2\ \cdots\ g_a] = \left(\boldsymbol{U}_{1:a}{}^{\mathrm{T}}\tilde{\boldsymbol{p}}\right)^{\mathrm{T}} \tag{9}$$

where a is the number of PCs satisfying $a < m$, and $\boldsymbol{U}_{1:a}{}^{\mathrm{T}} = [\boldsymbol{u}_1\ \boldsymbol{u}_2\ \cdots\ \boldsymbol{u}_a]^{\mathrm{T}}$ is called loading matrix or model projection matrix. The sample covariance matrix of the PCs $g_1\ g_2\ \cdots\ g_a$ is a diagonal matrix with the diagonal elements as $\lambda_1\ \lambda_2\ \cdots\ \lambda_a$.

Concurrently, a vector of RVs can be obtained by:

$$\boldsymbol{e}^{\mathrm{T}} = [e_1\ e_2\ \cdots\ e_m] = \left(\tilde{\boldsymbol{p}} - \boldsymbol{U}_{1:a}\boldsymbol{U}_{1:a}{}^{\mathrm{T}}\tilde{\boldsymbol{p}}\right)^{\mathrm{T}} \tag{10}$$

As for the determination of the number a of PCs, the Cumulative Percent Variance (CPV) criterion, widely used in multivariate statistical monitoring [32]-[34], is adopted. For the specific case here, CPV can be calculated as:

$$\mathrm{CPV}(a) = \frac{\sum_{i=1}^{a}\lambda_i}{\sum_{i=1}^{m}\lambda_i} \times 100\% \tag{11}$$

where a can be determined once $\mathrm{CPV}(a)$ exceeds a pre-defined constant. Typically, $\mathrm{CPV}(a) >= 90\%$ is sufficient to signify that most variable variances are captured by PCs and the remaining tiny variances are captured by RVs [33].

A measure of the variation within the PCA model can be given by the Hotelling's T^2 statistic as:

$$T^2 = \boldsymbol{g}^{\mathrm{T}}\boldsymbol{\Omega}\boldsymbol{g} = \sum_{i=1}^{a}\left(g_i/\sqrt{\lambda_i}\right)^2 \tag{12}$$

where $\boldsymbol{\Omega}$ is a diagonal matrix with the diagonal elements as $\lambda_1^{-1}, \lambda_2^{-1}, \cdots, \lambda_a^{-1}$.

Besides, a measure of the variation in the residual space not accounted for by the PCA model can be given by the companion Squared Prediction Error (SPE) statistic as:

$$\mathrm{SPE} = \boldsymbol{e}^{\mathrm{T}}\boldsymbol{e} = \sum_{i=1}^{m}e_i^2 \tag{13}$$

It can be found from (12) and (13) that T^2 and SPE are complementary to each other. Owing to such complementary nature of these two indices, a unified index is obtained here by incorporating T^2 with SPE as follows:

$$H = \eta T^2 + (1-\eta)\mathrm{SPE} \tag{14}$$

where η is a weighted coefficient satisfying $0 \le \eta \le 1$. The advantages of the built H statistic are that it can not only reduce the real-time monitoring burden but also can provide more comprehensive information. The parameter η is used to adjust the proportion of T^2 and SPE in H. If $\eta = 0$, H reduces to SPE; if $\eta = 1$, H reduces to T^2. Here, η is determined so that T^2 and SPE can be considered equivalent in H. The determination strategy is inspired by [35], where a combinatorial optimization problem was considered and the weightings of different sub-objective functions were unified through the comparison of matrix spectral radiuses. Thus, matrix spectral radiuses are introduced to help determine η. More specifically, (14) can be further written as follows:

$$H = \eta\tilde{\boldsymbol{p}}^{\mathrm{T}}\left(\boldsymbol{U}_{1:a}\boldsymbol{\Omega}\boldsymbol{U}_{1:a}{}^{\mathrm{T}}\right)\tilde{\boldsymbol{p}} + (1-\eta)\tilde{\boldsymbol{p}}^{\mathrm{T}}\left(\mathbf{I} - \boldsymbol{U}_{1:a}\boldsymbol{U}_{1:a}{}^{\mathrm{T}}\right)\tilde{\boldsymbol{p}} \tag{15}$$

where $\mathbf{I}$ denotes the $m \times m$ identity matrix.

Then, the following equation is formed to determine η:

$$\eta\gamma\left(\boldsymbol{U}_{1:a}\boldsymbol{\Omega}\boldsymbol{U}_{1:a}{}^{\mathrm{T}}\right) = (1-\eta)\gamma\left(\mathbf{I} - \boldsymbol{U}_{1:a}\boldsymbol{U}_{1:a}{}^{\mathrm{T}}\right) \tag{16}$$

where $\gamma(\Theta)$ denotes the spectral radius of Θ, calculated as the largest absolute value of the eigenvalues of Θ.

The solution to (16) is given by:

$$\eta_{bal} = \frac{\gamma\left(\mathbf{I} - \boldsymbol{U}_{1:a}\boldsymbol{U}_{1:a}{}^{\mathrm{T}}\right)}{\gamma\left(\boldsymbol{U}_{1:a}\boldsymbol{\Omega}\boldsymbol{U}_{1:a}{}^{\mathrm{T}}\right) + \gamma\left(\mathbf{I} - \boldsymbol{U}_{1:a}\boldsymbol{U}_{1:a}{}^{\mathrm{T}}\right)} \tag{17}$$

where $\eta_{bal} < \eta \le 1$ means T^2 is considered more important

than SPE, while $0 \le \eta < \eta_{bal}$ means T^2 is considered less important than SPE. Thus, η_{bal} is used in the expression of H to balance the weightings of T^2 and SPE.

After the construction of the H statistic, a detection threshold H^α with the confidence level of α is required for judging whether an active power event occurs or not. Since no prior knowledge is available with regard to the distributions of the monitored variables and the H statistic, a data-dependent strategy is given here, which determines H^α as the δth highest value of $\{H_n\}_{n=1}^N$, where δ is the integer nearest to $N(1-\alpha)$.

Thus, the PCA model for multivariate analysis of active power and the comprehensive statistic H for event detection have been built. Next, event localization will be introduced.

B. Event localization

After event detection provides the time when energy should be stored by ESSs or returned back to a power grid, event localization is the subsequent step that identifies the buses where an active power event occurs and determines appropriate locations of ESSs which should take action.

According to [36], contribution plots can reveal the variables that make the highest contribution to the detected anomaly or event and thus can help identify the event location. In the context of the stated problem here, a contribution plot strategy is built based on the sensitivity analysis [37], which calculates the rates of change in the system output variables resulting from small perturbations in parameters of interest. More specifically, the contributions of the normalized variables $\tilde{p}_1\ \tilde{p}_2\ \cdots\ \tilde{p}_m$ to the H statistic are defined and calculated by:

$$\mathbf{con}^{\mathrm{T}} = [\mathrm{con}_1 \quad \mathrm{con}_2 \quad \cdots \quad \mathrm{con}_m] = \frac{dH}{d\tilde{\boldsymbol{p}}^{\mathrm{T}}} \circ \tilde{\boldsymbol{p}}^{\mathrm{T}} = \left(2\tilde{\boldsymbol{p}}^{\mathrm{T}}\left(\eta_{bal}\boldsymbol{U}_{1:a}\boldsymbol{\Omega}\boldsymbol{U}_{1:a}{}^{\mathrm{T}} + (1-\eta_{bal})\left(\mathbf{I} - \boldsymbol{U}_{1:a}\boldsymbol{U}_{1:a}{}^{\mathrm{T}}\right)\right)\right) \circ \tilde{\boldsymbol{p}}^{\mathrm{T}} \tag{18}$$

where the ith entry con_i denotes the contribution of $\tilde{p}_i$ to H, "$\circ$" denotes the element-by-element multiplication of two vectors, and d denotes the derivative operator.

The signs of the contributions of the variables to the H statistic can be positive or negative. Usually, the signs of the contributions are not important whereas the absolute values indicate the effect of variables on a monitoring statistic. Moreover, the contributions of different variables have different means and variances, which can result in inaccurate identification results. This problem can be solved using the mean and variance of the contributions of each variable calculated from the normalized modelling data to scale the present contribution of the corresponding variable. Based on the above analysis, the procedure of event localization using the built contribution plot strategy is summarized as follows:

① The contributions $\{\mathbf{con}_n\}_{n=1}^N$ of the normalized variables $\tilde{p}_1\ \tilde{p}_2\ \cdots\ \tilde{p}_m$ are calculated by (18) based on the normalized modelling data $\{\tilde{\boldsymbol{p}}_n\}_{n=1}^N$.

② The sample means and sample standard deviations of the obtained contributions $\{\mathbf{con}_n\}_{n=1}^N$ are calculated.

③ Suppose that an active power event is detected by the H statistic at the kth sampling time point. The contributions $\mathbf{con}_k$ are obtained by (18) and scaled with the sample means and sample variances calculated from ②.

④ The absolute values of the scaled contributions, denoted by $\mathbf{con}_k{}^*$, are then used to identify the variables that make the largest contributions to the detected event.

Thus, the PCA based WAM method has been developed. With this method, the grid information about when and where electrical energy needs to be stored or returned back can be captured to guide the operation of ESSs. The flow chart for implementation is shown in Fig. 4.

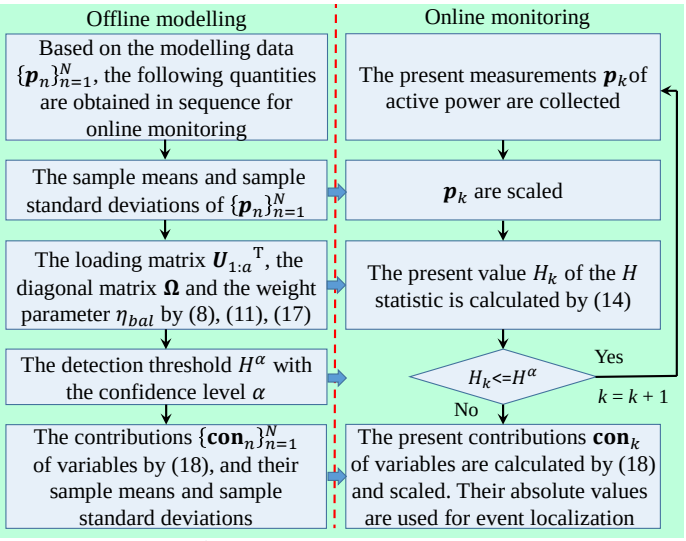

Fig. 4. The procedure of the PCA based WAM method.

V. Simulation Results and Analysis

This section investigates the potential of WAM in coordinating a power grid and ESSs as well as the benefit of ESSs on a power grid using a test model specifically built for a UK power grid enhanced with lithium-ion battery ESSs and multivariate statistical analysis based WAM. In the following, a reduced equivalent model of the UK power grid will be described firstly, followed by two test scenarios with the detailed analysis which are a change in the active power of a load bus and a change in the active power of a wind generator bus.

A. Reduced equivalent model of the UK power grid

A reduced equivalent model of the UK power grid, referred to as RUKG, is described here. A single-line diagram of RUKG with 29 nodes inter-connected through transmission lines is shown in Fig. 5. The skeleton for RUKG is obtained from a model of the power flow in the UK power grid developed at the University of Strathclyde [38]. Based on this skeleton, another reduced equivalent model of the UK power grid was developed in [39]. However, the model in [39] contains the dynamic representation of the generation mix while the transmission network and loads are represented together by the impedance matrix. In comparison, RUKG models the generation mix and represents the loads separately from the impedance matrix of the transmission network.

Taking [40] as the main source of reference data along with a variety of generator operators' web sites, the expected generation level in 2023 called 2023 scenario was described in [39]. In this scenario, different types of generation are distributed

across 29 nodes, as shown in Fig. 5. Here, the generation mix of RUKG is the same as that of the 2023 scenario, which has already been described previously in Section II-A. The detailed generation locations and capacities, and the formula for calculating these capacities can be further found in [39].

In total, there are 36 synchronous generator buses (10-coal, 7-nuclear, 5-hydro and 14-CCGT), 15 wind generator buses and 29 load buses in RUKG. The base transmission network is shown in Fig. 5.

Table I lists the ESS locations (the nodes where ESSs are placed and the wind generator buses to which ESSs are connected) and the synchronous generator buses whose frequencies are used as the control objective variables, where G_i denotes the ith generator bus.

Table II lists all of the monitored variables and the nodes where they are located. Firstly, 500 modelling data points are obtained in the ambient condition with the sample interval of 0.1 seconds. The number a of PCs is determined as 32 by (11) and the parameter η_{bal} is determined as 0.443 by (17).

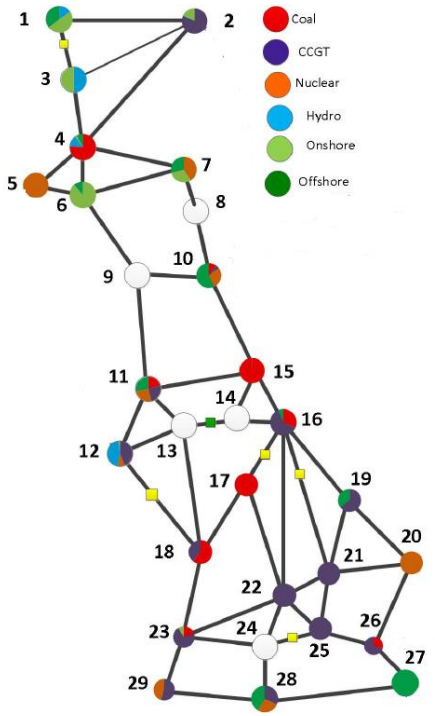

Fig. 5. A single-line diagram of RUKG [39].

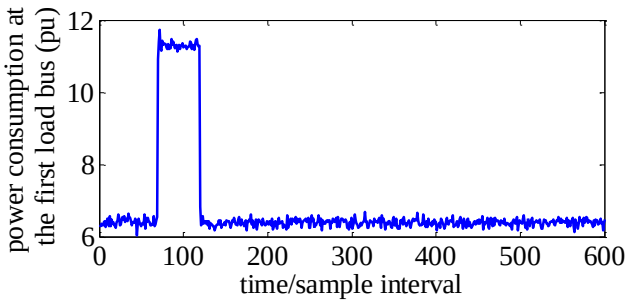

Fig. 6. A change in the active power of the first load bus L_1.

TABLE I
THE ESS LOCATIONS AND THE BUSES WHOSE FREQUENCIES ARE USED AS CONTROL OBJECTIVE VARIABLES

Node / Buses	Buses to which ESSs are connected	Buses whose frequencies are taken as control objective variables
1 / G_1 G_2	G_1 (W_1)	G_2 (S_1)
2 / G_3-G_5	G_4 (W_2)	G_3 (S_2)
3 / G_6 G_7	G_6 (W_3)	G_7 (S_4)
4 / G_8-G_{10}	G_9 (W_4)	G_8 (S_5)
6 / G_{12}	G_{12} (W_5)	G_{11} (S_7)
7 / G_{13} G_{14}	G_{14} (W_6)	G_{13} (S_8)
10 / G_{15}-G_{18}	G_{18} (W_7)	G_{17} (S_{11})
11 / G_{19}-G_{22}	G_{22} (W_8)	G_{21} (S_{14})
12 / G_{23}-G_{26}	G_{25} (W_9)	G_{23} (S_{15})
15 / G_{27} G_{28}	G_{28} (W_{10})	G_{27} (S_{18})
16 / G_{29}-G_{31}	G_{31} (W_{11})	G_{29} (S_{19})
19 / G_{35} G_{36}	G_{36} (W_{12})	G_{35} (S_{24})
23 / G_{40}-G_{42}	G_{42} (W_{13})	G_{40} (S_{28})
27 / G_{46}	G_{46} (W_{14})	G_{47} (S_{33})
29 / G_{49}-G_{51}	G_{49} (W_{15})	G_{50} (S_{35})

TABLE II
THE MONITORED VARIABLES AND THE NODES WHERE THEY ARE MEASURED

Node	Active Power	Node	Active Power	Node	Active Power
1	p_{W_1} of G_1		$p_{W_{10}}$ of G_{28}	4	p_{L_4} of L_4
	p_{S_1} of G_2	16	$p_{S_{19}}$ of G_{29}	5	p_{L_5} of L_5
2	p_{S_2} of G_3		$p_{S_{20}}$ of G_{30}	6	p_{L_6} of L_6
	p_{W_2} of G_4		$p_{W_{11}}$ of G_{31}	7	p_{L_7} of L_7
	p_{S_3} of G_5	17	$p_{S_{21}}$ of G_{32}		p_{L_8} of L_8
3	p_{W_3} of G_6	18	$p_{S_{22}}$ of G_{33}	10	p_{L_9} of L_9
	p_{S_4} of G_7		$p_{S_{23}}$ of G_{34}		$p_{L_{10}}$ of L_{10}
4	p_{S_5} of G_8	19	$p_{S_{24}}$ of G_{35}	11	$p_{L_{11}}$ of L_{11}
	p_{W_4} of G_9		$p_{W_{12}}$ of G_{36}	12	$p_{L_{12}}$ of L_{12}
	p_{S_6} of G_{10}	20	$p_{S_{25}}$ of G_{37}		$p_{L_{13}}$ of L_{13}
5	p_{S_7} of G_{11}	21	$p_{S_{26}}$ of G_{38}	15	$p_{L_{14}}$ of L_{14}
6	p_{W_5} of G_{12}	22	$p_{S_{27}}$ of G_{39}		$p_{L_{15}}$ of L_{15}
7	p_{S_8} of G_{13}	23	$p_{S_{28}}$ of G_{40}	16	$p_{L_{16}}$ of L_{16}
	p_{W_6} of G_{14}		$p_{S_{29}}$ of G_{41}	17	$p_{L_{17}}$ of L_{17}
10	p_{S_9} of G_{15}		$p_{W_{13}}$ of G_{42}	18	$p_{L_{18}}$ of L_{18}
	$p_{S_{10}}$ of G_{16}	25	$p_{S_{30}}$ of G_{43}	19	$p_{L_{19}}$ of L_{19}
	$p_{S_{11}}$ of G_{17}	26	$p_{S_{31}}$ of G_{44}	20	$p_{L_{20}}$ of L_{20}
	p_{W_7} of G_{18}		$p_{S_{32}}$ of G_{45}	21	$p_{L_{21}}$ of L_{21}
11	$p_{S_{12}}$ of G_{19}	27	$p_{W_{14}}$ of G_{46}	22	$p_{L_{22}}$ of L_{22}
	$p_{S_{13}}$ of G_{20}	28	$p_{S_{33}}$ of G_{47}	23	$p_{L_{23}}$ of L_{23}
	$p_{S_{14}}$ of G_{21}		$p_{S_{34}}$ of G_{48}		$p_{L_{24}}$ of L_{24}
	p_{W_8} of G_{22}	29	$p_{W_{15}}$ of G_{49}	25	$p_{L_{25}}$ of L_{25}
12	$p_{S_{15}}$ of G_{23}		$p_{S_{35}}$ of G_{50}	26	$p_{L_{26}}$ of L_{26}
	$p_{S_{16}}$ of G_{24}		$p_{S_{36}}$ of G_{51}	27	$p_{L_{27}}$ of L_{27}
	p_{W_9} of G_{25}	1	p_{L_1} of L_1	28	$p_{L_{28}}$ of L_{28}
	$p_{S_{17}}$ of G_{26}	2	p_{L_2} of L_2	29	$p_{L_{29}}$ of L_{29}
15	$p_{S_{18}}$ of G_{27}	3	p_{L_3} of L_3		

B. *Change in the active power of a load bus*

A representative change in the active power of the first load bus L_1 is simulated and shown in Fig. 6, where the power change occurs at the 70th sampling time point and lasts for 50 sampling time points.

The WAM chart for this scenario is shown in Fig. 7. The confidence level is set as $\alpha = 99\%$. It can be seen from the upper subfigure that the H statistic detects the event at the 70th sampling time point and from the lower subfigure that the contributions plot $\mathbf{con}_{70}{}^{*}$ identifies the 52nd variable as the one making the largest contribution to the detected event. It can

be understood from (7) together with Table II that the identified variable is exactly the active power at the first load bus L_1. With Fig. 7, the event information is captured for ESSs. Accordingly, the ESS connected to the first wind generator bus G_1 (W_1) is switched on to discharge when the event is detected. The reason is that L_1 is directly connected with G_1 (W_1) by a transmission line. Moreover, the frequency of the first synchronous generator bus G_2 (S_1) which is near G_1 (W_1) is used as the control objective variable with the set point of 50 Hz. Thus, the way in which a power grid and ESSs can be coordinated by the developed WAM approach, which is the main consideration of this paper, is illustrated. Due to such coordination, a response in which only ESSs near the target area charge or discharge is enabled and a reduced impact on the grid stability can be achieved.

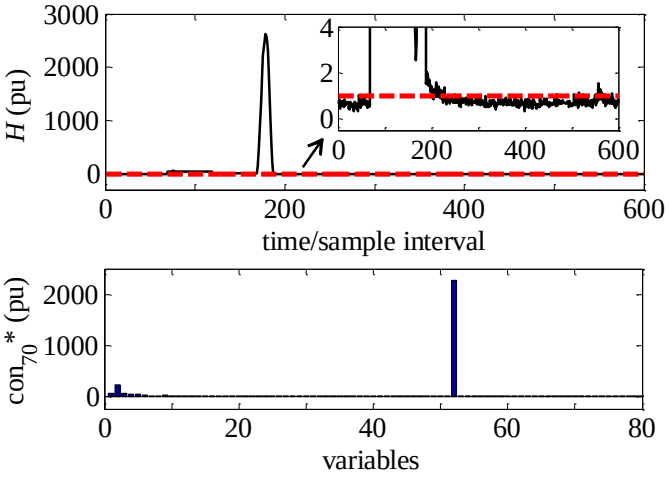

Fig. 7. The WAM chart for the first test scenario.

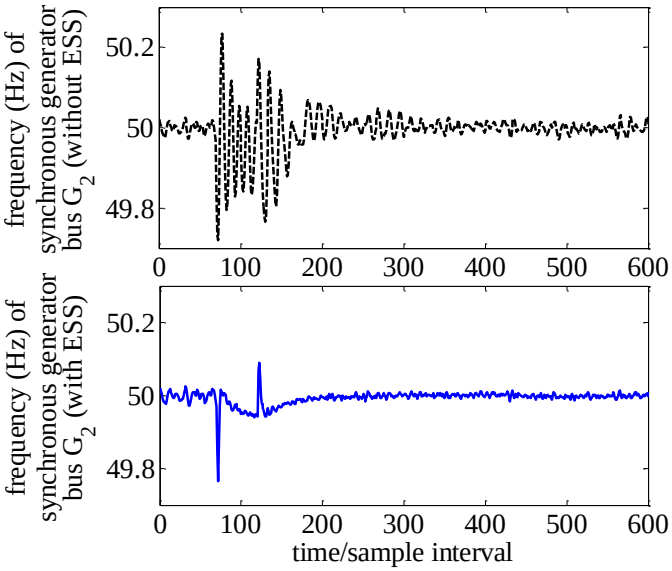

Fig. 8. The time trend of the frequency of the synchronous generator bus G_2 (S_1) under the condition without ESS and the condition with the ESS designated by WAM.

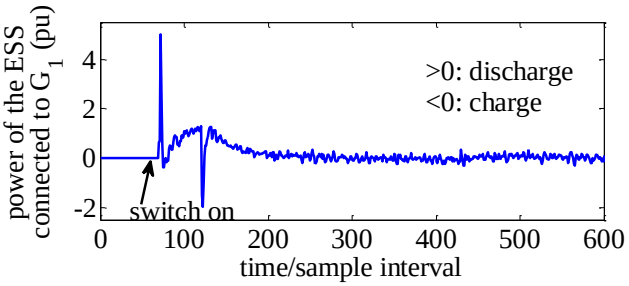

Fig. 9. The operation of the ESS connected to the wind generator bus G_1 (W_1) under the condition with the ESS designated by WAM.

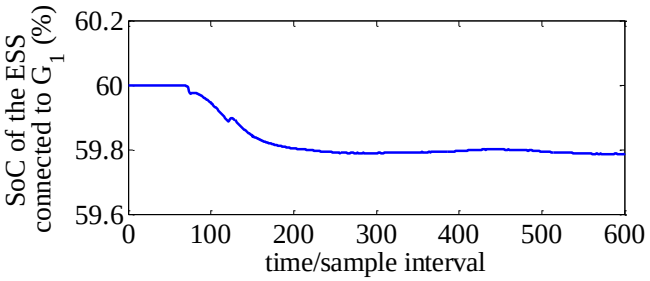

Fig. 10. The tracked SoC of the ESS connected to the wind generator bus G_1 (W_1) under the condition with the ESS designated by WAM.

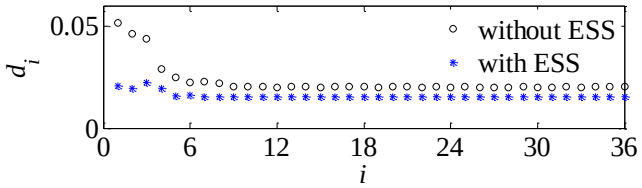

Fig. 11. The calculation results of the index d_i measuring the deviation of the frequency f_i from nominal frequency for i from 1 to 36 in the first test scenario.

Fig. 8 shows the time trend of the frequency of G_2 (S_1), where the frequency under the condition with the ESS designated by WAM is more stable than that under the condition without ESS.

Fig. 9 illustrates the operation of the ESS connected to G_1 (W_1). It shows a spike at about the 70th sampling time point, indicating rapid discharge to supply the power when the step-up power change in L_1 occurs. It also shows an opposite spike at about the 120th sampling time point, indicating rapid charge to absorb the power when the power change in L_1 ends. An interesting point is that the time trend in Fig. 9 is approximately inverse from that in the lower subfigure of Fig. 8. This is reasonable because the proportional control scheme is used, as shown in Fig. 3.

With the energy of the ESS connected to G_1 (W_1) flowing in and out for frequency regulation as illustrated in Fig. 9, the State of Charge (SoC) of the designated ESS varies as shown in Fig. 10, where the initial SoC is 60%. It can be observed from Fig. 10 that a small amount of the energy stored in the designated ESS is consumed over the frequency regulation period and the stored energy is sufficient for response to the frequency deviation in this test scenario.

The time trends of the frequencies of the other 35 synchronous generator buses under the condition with the ESS designated by WAM are also more stable than those of the corresponding synchronous generator buses under the condition

without ESS. For a succinct description, the time trends of the other 35 frequencies are not shown here. Instead, an index that can measure the deviation of the time trend of the frequency of a synchronous generator bus from the nominal frequency (50Hz in this case study) is defined below:

$$d_i = \sqrt{\frac{1}{K-1}\sum_{k=1}^{K}\left(f_{i,k} - 50\right)^2} \quad (19)$$

where K denotes the number of the frequency samples, f_i denotes the frequency of the ith synchronous generator bus S_i, and $f_{i,k}$ denotes the value of f_i at the kth sampling time point.

Fig. 11 shows the index d_i for i from 1 to 36 under the condition without ESS and the condition with the ESS designated by WAM, where d_i under the condition with the designated ESS is smaller than that under the condition without ESS. Thus, the results in Fig. 11 and Fig. 8 illustrate the benefit of the ESS designated by WAM for frequency stability.

C. *Change in the active power of a wind generator bus*

A representative change in the active power of the third wind generator bus G_6 (W_3) is simulated, as shown in Fig. 12, where the power loss occurs at the 71st sampling time point and lasts for 50 sampling time points.

Fig. 13 shows the WAM chart for this scenario. The H statistic in the upper subfigure gives a definite indication of the event at the 71st sampling time point and the contributions plot $\mathbf{con}_{71}{}^*$ in the lower subfigure indicates the 39th variable contributes most to the detected event. Referring to (7) and Table II, the 39th variable is exactly the active power at the third wind generator bus G_6 (W_3). Thus, the ESS connected to G_6 (W_3) is switched on to discharge when the event is detected and the frequency of the synchronous generator bus G_7 (S_4) which is near G_6 (W_3) is taken as the control objective variable. Again, the way in which the developed WAM method coordinates a power grid and ESSs, which is the main concern within this paper, is demonstrated.

Fig. 14 shows the time trend of the frequency of G_7 (S_4), where the frequency under the condition with the ESS designated by WAM is also more stable than that under the condition without ESS, especially for the duration of the wind power loss.

The operation of the ESS connected to G_6 (W_3) is shown in Fig. 15, illustrating the ESS discharges rapidly to compensate for the power loss when the step-down power change in G_6 (W_3) occurs and it charges rapidly when the power change in G_6 (W_3) ends. Besides, the time trend in Fig. 15 is also approximately inverse from that in the lower subfigure of Fig. 14.

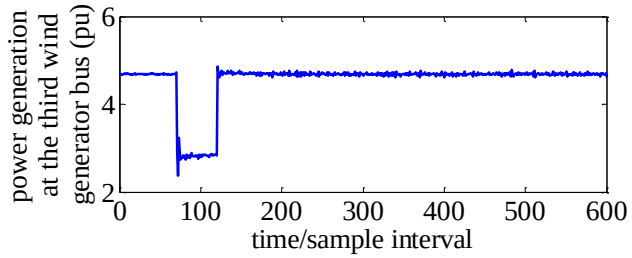

Fig. 12. The change in the active power of the third wind generator bus G_6 (W_3).

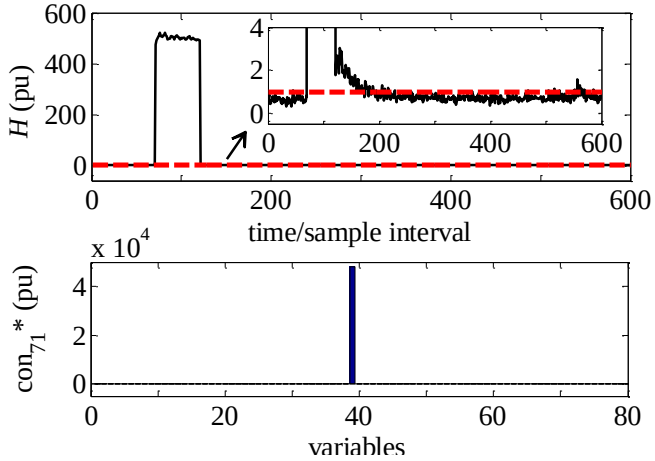

Fig. 13. The WAM chart for the second test scenario.

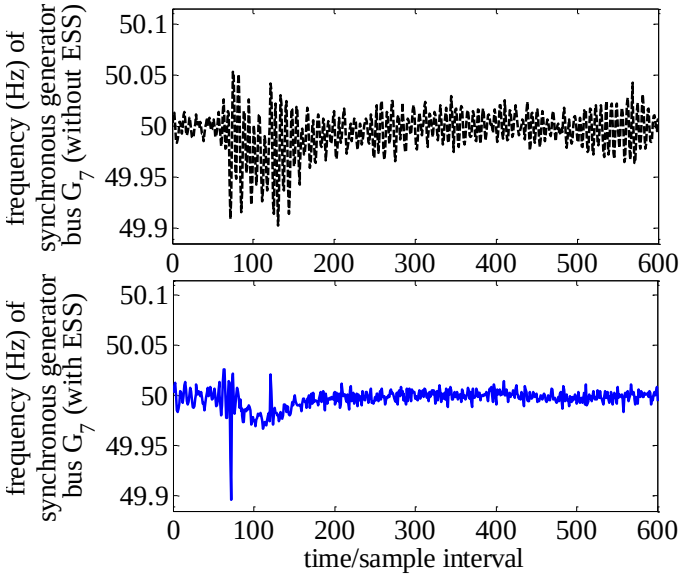

Fig. 14. The time trend of the frequency of the synchronous generator bus G_7 (S_4) under the condition without ESS and the condition with the ESS designated by WAM.

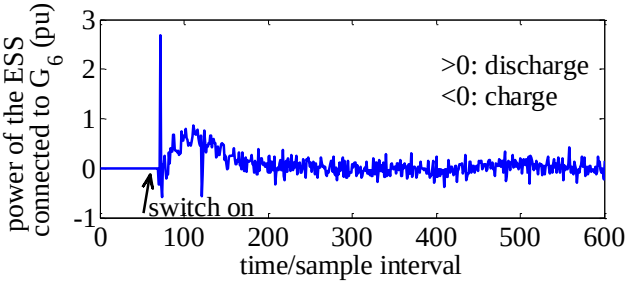

Fig. 15. The operation of the ESS connected to the wind generator bus G_6 (W_3) under the condition with the ESS designated by WAM.

Fig. 16 illustrates the tracked SoC of the ESS connected to the wind generator bus G_6 (W_3), where the initial SoC is also 60%. Similar to the tracked SoC of Fig. 10 in the first test scenario, the consumed energy from the designated ESS over the frequency regulation period is also in a small amount and the energy stored in the designated ESS is also adequate for restraining the frequency deviation in this test scenario.

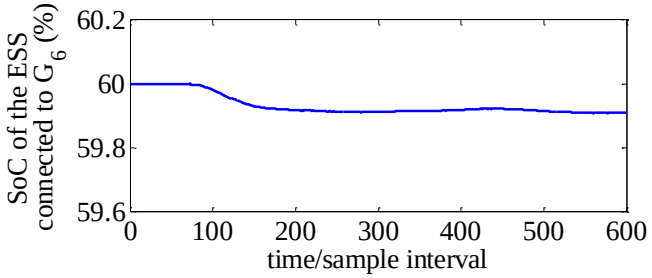

Fig. 16. The tracked SoC of the ESS connected to the wind generator bus G_6 (W_3) under the condition with the ESS designated by WAM.

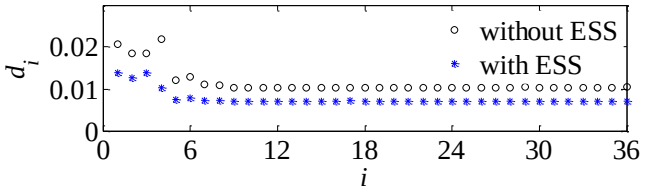

Fig. 17. The calculation results of the index d_i measuring the deviation of the frequency f_i from nominal frequency for i from 1 to 36 in the second scenario.

Fig. 17 shows the index d_i for i from 1 to 36 under the condition without ESS and the condition with the ESS designated by WAM. It can be seen from Fig. 17 that d_i under the condition with the designated ESS is also smaller than that under the condition without ESS. This means the deviation of f_i from the nominal frequency under the condition with the designated ESS is smaller than that under the condition without ESS. Thus, the results in Fig. 17 and Fig. 14 illustrate that the ESS designated by WAM improves frequency stability.

VI. Discussions

Besides the above simulation results and analysis based on the test model, there are three interesting additional features regarding this model which are worthwhile to be discussed here. The first one is about the generalizability of the test model. Because the power grid model, the battery ESSs model and the WAM model constituting the test model were developed separately with no mutually exclusive constraints before connection, they can be conveniently substituted with models of other power grids or energy storage techniques, making the test model adaptable and generalizable.

Another feature is about the dependence of the WAM method on the measurement coverage. If a location where a disturbance occurs were not covered by measuring devices, the WAM model would not be able to detect and locate the disturbance for guiding the operation of battery ESSs due to the lack of disturbance information in the measured data, resulting in a larger frequency deviation. Fortunately, the measurement coverage is being extended constantly with more and more measuring devices added across power systems. Besides, a strategy for optimal sensor placement in [41] is a feasible solution if wide measurement coverage cannot be achieved in some cases.

The third aspect is about the implicit assumption of the test model that the energy in the ESS designated by the WAM method is sufficient for response to the frequency deviation. Since the energy of the designated ESS keeps flowing in and out for frequency regulation, usually a small amount of energy is required over the regulation period and the assumption can usually be met. Thus, the designated ESS can be observed to provide fast primary frequency response which is required from a system with continuous drop in inertial response. If sometimes a large amount of energy were required, e.g., in the case of a major outage or loss of a large generator, it would be desirable to develop a control method explicitly considering the energy available in the designated ESS and appropriately modifying the gains so that energy depletion can be avoided while supporting the power grid operation. Developing such a control method is outside the scope of the present work, but will be investigated in future research following the present work.

VII. Conclusions

A Wide-Area Monitoring (WAM) method has been developed based on multivariate statistical analysis and a test model has been presented for investigating how WAM can coordinate a power grid and Energy Storage Systems (ESSs). Simulation studies using the reduced equivalent model specifically built for a UK power grid enhanced with lithium-ion battery ESSs and WAM have been conducted. The simulation results have demonstrated that the developed WAM approach plays an important role in coordinating a power grid and battery ESSs by capturing the grid information to guide the operation of ESSs, and ESSs effectively improve frequency stability with the support of WAM.

Acknowledgment

The authors acknowledge Dr. Linash P. Kunjumuhammed of the Power and Control Group, Imperial College London for providing a reduced equivalent model of the UK power grid, and acknowledge Dr. David A. Howey of the Energy and Power Group, University of Oxford for providing a lithium-ion battery cell model to support this paper.

References

[1] Climate Change Act 2008, "Carbon targeting and budgeting, Chapter 27, Part 1—The target for 2050," *UK: Her Majesty's Stationery Office Limited*, 2008.

[2] Directive 2009/28/EC of the European Parliament and of the COUNCIL, "On the promotion of the use of energy from renewable sources and amending and subsequently repealing Directives 2001/77/EC and 2003/30/EC," *Official Journal of the European Union*, Apr. 2009.

[3] Nationalgrid, "Electricity Ten Year Statement 2016—UK electricity transmission," Nov. 2016.

[4] P. M. Ashton, C. S. Saunders, G. A. Taylor, A. M. Carter, and M. E. Bradley, "Inertia estimation of the GB power system using synchrophasor measurements," *IEEE Trans. Power Syst.*, vol. 30, no. 2, pp. 701-709, Mar. 2015.

[5] X. Luo, J. Wang, M. Dooner, and J. Clarke, "Overview of current development in electrical energy storage technologies and the application potential in power system operation," *Appl. Energy*, vol. 137, pp. 511-536, Jan. 2015.

[6] H. Zhao, Q. Wu, S. Hu, H. Xu, and C. N. Rasmussen, "Review of energy storage system for wind power integration support," *Appl. Energy*, vol. 137, pp. 545-553, Jan. 2015.

[7] Y. Liu, W. Du, L. Xiao, H. Wang, and J. Cao, "A method for sizing energy storage system to increase wind penetration as limited by grid frequency deviations," *IEEE Trans. Power Syst.*, vol. 31, no. 1, pp. 729-737, Jan. 2016.

[8] B. Lian, A. Sims, D. Yu, C. Wang., and R. W. Dunn, "Optimizing LiFePO4 battery energy storage systems for frequency response in the UK system," *IEEE Trans. Sustain. Energy*, vol. 8, no. 1, pp. 385-394, Jan. 2017.

[9] K. Hartwig and I. Kockar, "Impact of strategic behavior and ownership of energy storage on provision of flexibility," *IEEE Trans. Sustain. Energy*, vol. 7, no. 2, pp. 744-754, Apr. 2016.
[10] A. Castillo and D. F. Gayme, "Grid-scale energy storage applications in renewable energy integration: A survey," *Energy Conversion and Management*, vol. 87, pp. 885-894, Nov. 2014.
[11] D. F. Gayme and U. Topcu, "Optimal power flow with large-scale storage integration," *IEEE Trans. Power Syst*., vol. 28, no. 2, pp. 709-717, May 2013.
[12] S. Wogrin and D. F. Gayme, "Optimizing storage siting, sizing, and technology portfolios in transmission-constrained networks," *IEEE Trans. Power Syst.*, vol. 30, no. 6, pp. 3304-3313, Nov. 2015.
[13] H. Pandžić, Y. Wang, T. Qiu, Y. Dvorkin, and D. S. Kirschen, "Near-optimal method for siting and sizing of distributed storage in a transmission network," *IEEE Trans. Power Syst.*, vol. 30, No. 5, pp. 2288-2300, Sept. 2015.
[14] Y. Dvorkin, R. Fernández-Blanco, D. S. Kirschen, H. Pandžić, J. Watson, and C. A. Silva-Monroy, "Ensuring profitability of energy storage," *IEEE Trans. Power Syst.*, vol. 32, no. 1, pp. 611-623, Jan. 2017.
[15] M. R. Almassalkhi *et al*., "Incorporating storage as a flexible transmission asset in power system operation procedure," in *Proc. Power Systems Computation Conference (PSCC)*, Genoa, Italy, Jun. 2016, pp. 1-7.
[16] J. A. Martin and I. A. Hiskens, "Corrective model-predictive control in large electric power systems," *IEEE Trans. Power Syst*., vol. 32, no. 2, pp. 1651-1662, Mar. 2017.
[17] H. Khani, M. R. Dadash Zadeh, and A. H. Hajimiragha, "Transmission congestion relief using privately owned large-scale energy storage systems in a competitive electricity market," *IEEE Trans. Power Syst.*, vol. 31, no. 2, pp. 1449-1458, Mar. 2016.
[18] A. Farraj, E. Hammad, and D. Kundur, "On the use of energy storage systems and linear feedback optimal control for transient stability," *IEEE Trans. Industrial Informatics*, vol. 13, no. 4, pp. 1575-1585, Aug. 2017.
[19] J. W. Choi, S. Y. Heo, and M. K. Kim, "Hybrid operation strategy of wind energy storage system for power grid frequency regulation," *IET Gener. Transm. Distrib*., vol. 10, no. 3, pp. 736-749, Mar. 2016.
[20] D. M. Greenwood, K. Y. Lim, C. Patsios, P. F. Lyons, Y. S. Lim, and P. C. Taylor, "Frequency response services designed for energy storage," *Appl. Energy*, vol. 203, pp. 115-127, Oct. 2017.
[21] L. S. Vargas, G. Bustos-Turu, and F. Larraín, "Wind power curtailment and energy storage in transmission congestion management considering power plants ramp rates," *IEEE Trans. Power Syst*., vol. 30, no. 5, pp. 2498-2506, Sept. 2015.
[22] Z. Shu and P. Jirutitijaroen, "Optimal operation strategy of energy storage system for grid-connected wind power plants," *IEEE Trans. Sustain. Energy*, vol. 5, no. 1, pp. 190-199, Jan. 2014.
[23] A. Lucas and S. Chondrogiannis, "Smart grid energy storage controller for frequency regulation and peak shaving, using a vanadium redox flow battery," *International Journal of Electrical Power & Energy Systems*, vol. 80, pp. 26-36, Sept. 2016.
[24] C. Napoli, G. Pappalardo, G. M. Tina, and E. Tramontana, "Cooperative strategy for optimal management of smart grids by wavelet RNNs and cloud computing," *IEEE Trans. Neural Netw. Learn. Syst.*, vol. 27, no. 8, pp. 1672-1685, Aug. 2016.
[25] Á. Ortega and F. Milano, "Modeling, simulation, and comparison of control techniques for energy storage systems," *IEEE Trans. Power Syst*., vol. 32, no. 3, pp. 2445-2454, May 2017.
[26] IEC, "Electrical energy storage white paper," Tech. report, 2011.
[27] P. Kundur, *Power System Stability and Control*. New York, NY, USA: McGraw-Hill, 1994.
[28] WECC Renewable Energy Modeling Task Force, "WECC Wind Power Plant Dynamic Modeling Guide," WECC, Tech. Rep., Nov. 2010.
[29] C. R. Birkl and D. A. Howey, "Model identification and parameter estimation for LiFePO4 batteries," in *Proc. IET Hybrid and Electric Vehicles Conference (HEVC)*, London, U.K., Nov. 2013, pp. 1-6.
[30] M. André, "The ARTEMIS European driving cycles for measuring car pollutant emissions," *Science of the total Environment*, vols. 334-335, pp. 73-84, Dec. 2004.
[31] J. A. Short, D. G. Infield, and L. L. Freris, "Stabilization of grid frequency through dynamic demand control," *IEEE Trans. Power Syst.*, vol. 22, no. 3, pp. 1284-1293, Aug. 2007.
[32] L. Cai, X. Tian, and S. Chen, "A process monitoring method based on noisy independent component analysis," *Neurocomputing*, vol. 127, pp. 231-246, Mar. 2014.
[33] G. Li, S. Qin, and D. Zhou, "A new method of dynamic latent-variable modeling for process monitoring," *IEEE Trans. Ind. Electron.*, vol. 61, no.11, pp. 6438-6445, Nov. 2014.
[34] W. Zhu *et al.*, "A novel KICA-PCA fault detection model for condition process of hydroelectric generating unit," *Measurement*, vol. 58, pp. 197-206, Dec. 2014.
[35] Q. Liu, X. Tang, H. Lu, and S. Ma, "Face recognition using kernel scatter-difference-based discriminant analysis," *IEEE Trans. Neural Netw.*, vol. 17, no. 4, pp. 1081-1085, Jul. 2006.
[36] L. Cai, X. Tian, and S. Chen, "Monitoring nonlinear and non-Gaussian processes using Gaussian mixture model-based weighted kernel independent component analysis," *IEEE Trans. Neural Netw. Learn. Syst.*, vol. 28, no. 1, pp. 122-135, Jan. 2017.
[37] L. Petzold, S. Li, Y. Cao, and R. Serban, "Sensitivity analysis of differential-algebraic equations and partial differential equations," *Comput. Chem. Eng.*, vol. 30, nos. 10-12, pp. 1553-1559, Sep. 2006.
[38] K. R. W. Bell and A. N. D. Tleis, "Test system requirements for modelling future power systems," in *Proc. IEEE Power and Energy Society General Meeting*, Providence, RI, USA, Jul. 2010, pp. 1-8.
[39] L. P. Kunjumuhammed, B. C. Pal, and N. F. Thornhill, "A test system model for stability studies of UK power grid," in *Proc. IEEE PowerTech*, Grenoble, France, Jun. 2013, pp. 1-6.
[40] Nationalgrid, "Electricity Ten Year Statement 2012," Nov. 2012.
[41] I. R. Cabrera, E. Barocio, R. J. Betancourt, and A. R. Messina, "A semi-distributed energy-based framework for the analysis and visualization of power system disturbances," *Electr. Power Syst. Res.*, vol. 143, pp. 339-346, Feb. 2017.

Lianfang Cai received the B.Eng. and Ph.D. degrees from China University of Petroleum, Qingdao, China, in 2009 and 2014, respectively. From 2015 until 2017, he worked as a Postdoctoral Research Associate at Imperial College London, UK. Presently he is a Project Engineer at University of Warwick, UK. His research interests include data-driven power system monitoring, simulation of power systems with energy storage, multivariate statistical modelling, and data analysis.

Nina F. Thornhill (SM'93) received the B.A. degree in physics from University of Oxford, Oxford, UK, in 1976, the M.Sc. degree from Imperial College London, UK, and the Ph.D. degree from University College London.
She is Professor of Process Automation in the Department of Chemical Engineering at Imperial College London where she holds the ABB Chair of Process Automation.

Stefanie Kuenzel (GS'11, M'14) received the M.Eng. and Ph.D. degrees from Imperial College London, London, UK, in 2010 and 2014, respectively. Presently she is the Head of the Power Systems Group and Lecturer in the Department of Electronic Engineering at Royal Holloway, University of London, and a visiting researcher at Imperial College London. Her current research interests include renewable generation and transmission, including HVDC.

Bikash C. Pal (M'00-SM'02-F'13) is Professor of Power Systems at Imperial College London. He is research active in power system stability, control and computation. Prof. Pal has graduated 20 PhDs and published 88 technical papers in IEEE Transactions and IET journals. He has co-authored two books and two awards winning IEEE Task Force/Working Group reports. He was Editor-in-Chief of IEEE Transactions on Sustainable Energy and Fellow of IEEE for his contribution to power system stability and control.